THE JOURNAL OF PHYSICAL CHEMISTRY A

Article

pubs.acs.org/JPCA

Absolute Measurement of Femtosecond Pump–Probe Signal Strength

Byungmoon Cho,[‡] Vivek Tiwari,[‡] Robert J. Hill,[§] William K. Peters,[#] Trevor L. Courtney,[†] Austin P. Spencer, and David M. Jonas*

Department of Chemistry and Biochemistry, University of Colorado, Boulder, Colorado 80309-0215, United States

ABSTRACT: The absolute femtosecond pump–probe signal strength of deprotonated fluorescein in basic methanol is measured. Calculations of the absolute pump–probe signal based on the steady-state absorption and emission spectrum that use only independently measured experimental parameters are carried out. The calculation of the pump–probe signal strength assumes the pump and probe fields are both weak and includes the following factors: the transverse spatial profile of the laser beams; the pulse spectra; attenuation of the propagating pulses with depth in the sample; the anisotropic transition probability for polarized light; and time-dependent electronic population relaxation. After vibrational and solvent relaxation are complete, the calculation matches the measurement to within 10% error without any adjustable parameters. This demonstrates quantitative measurement of absolute excited state population.

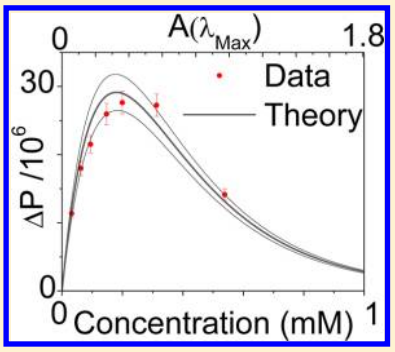

Absolute quantification of the concentration of excited electronic states is important for mechanistic and analytical investigations in chemistry. With flash photolysis, transient chemical species were generated and detected with a degree of control and accuracy,[1,2] enabling time-resolved investigation of radicals and other transient chemical species. Later, using actinometry, Porter and co-workers extended flash photolysis to measure the triplet yield of chlorophylls after photoexcitation;[3] chemical actinometry determined the fluence of the excitation flash and thus the absolute number of absorbed photons necessary for determination of the yield (for a recent description of actinometry, see ref 4). With the advent of pulsed lasers, flash photolysis has been superseded by the pump–probe technique.[5] Similar approaches work for pump–probe spectroscopy with nanosecond time resolution.[6] For picosecond pulses, time-dependent rotational alignment[5] must be considered for molecules in liquids.[7] For femtosecond pulses, the frequency dependence of the electronic transition probability becomes important.[8] The Z-scan technique can be used to absolutely determine spectrally averaged optical nonlinearities.[9−11] As in flash photolysis, relative absorption cross-sections and relative yields can be determined by global analysis of transient changes in the transmitted probe spectrum.[12] Estimates of signal strength can achieve a factor of 2 accuracy with rough approximations for spatial intensity variation and laser bandwidth.[13] However, a factor of 2 lies at the heart of phenomena such as multiple exciton generation[14] and singlet fission.[15] Here, calculation and measurement of the absolute pump–probe signal strength are described for a molecular system with well-characterized photophysics (the fluorescein dianion in basic methanol). Like the measurement of absolute triplet yields, measurement of pump and probe photon numbers and consideration of their attenuation as they propagate in the sample are required; however, treatments of the transverse spatial profiles of the laser beams, the polarization and frequency dependence of the excitation probabilities, and consideration of relaxation dynamics are also required.

In pump–probe experiments, the pump pulse excites a fraction of the ground state molecules into the excited state and a weak, time-delayed probe pulse interrogates the subsequent population change; the measured transient absorption signal discussed here is the pump-induced change in number of transmitted probe photons (or energy, depending on the detector) caused by the presence of the pump. An increase in the transmitted probe photon number is caused by depletion of the ground state population (ground state bleaching reduces probe attenuation) and stimulated emission from the excited state population (excited state emission amplifies the probe). If the excited state can make a transition to a higher excited state by absorbing a probe photon, this contribution reduces the transmitted probe intensity (excited state absorption). The net pump-induced change in the transmitted probe photon number from all three contributions is the pump–probe signal.

At early pump–probe delay, coherent electronic effects (typically lasting ∼100 fs in solution), coherent vibrational dynamics (wavepacket motion, typically lasting up to 10 ps in solution), and rotational coherence (typically lasting a few hundred picoseconds in solution) complicate the signal strength. To enable quantitative predictions with the fewest measured parameters, we focus on the pump–probe signal after enough time has elapsed so that electronic and vibrational

Special Issue: Prof. John C. Wright Festschrift

Received: February 25, 2013
Revised: April 6, 2013
Published: May 28, 2013

coherence can be neglected. After vibrational, rotational, and solvent relaxation, the pump−probe signal [the change in the transmitted photon number (probe energy) due to pump excitation] is directly related to Δn_g, the ground state population number density change, and Δn_e, the excited state population number density change (initially, $\Delta n_g = -\Delta n_e$). For weak excitation of dipolar transitions, nonequilibrium molecular rotational alignment can be phenomenologically incorporated without adjustable parameters via the polarization anisotropy. The effect of incomplete vibrational relaxation is more complicated and is not treated here, restricting the calculation to pump−probe delays large enough so that vibrational and solvent relaxation are complete (~20 ps for deprotonated fluorescein in basic methanol). The calculations are fundamentally based on Einstein's analysis of the kinetics of absorption and stimulated emission (B coefficients)[16−19] but mostly expressed in terms of experimentally accessible cross-sections. In the following section, we derive an expression for the pump−probe signal that is an explicit function of the cross-sections, which are functions of frequency.

THEORY

Femtosecond pump−probe spectroscopy involves spatially varying, time dependent, nonequilibrium level populations and angular alignment. The approach described here extends Beer's law in the differential form

$$\partial I(\boldsymbol{R}, \nu)/\partial Z = -n^0\sigma^0(\nu)I(\boldsymbol{R}, \nu) = -\alpha^0(\nu)I(\boldsymbol{R}, \nu) \quad (1)$$

where n^0 is the total equilibrium molecular number density, $\sigma^0(\nu)$ is the absorption cross-section of the equilibrium state, $\alpha^0(\nu)$ is the equilibrium absorption coefficient for the intensity[20] (to avoid confusion, it should be noted that an α that is a factor of 2 smaller is sometimes used to quantify attenuation of the field[21,22]), $I(\boldsymbol{R}, \nu)$ is the spectral intensity (or irradiance[23]) distribution of the light source, $\boldsymbol{R}$ is the spatial coordinate vector, and Z is the propagation direction. The beams are approximated as propagating with fixed transverse profiles (similar to the approximation of collimated Gaussian beams[24]). This approximation requires a sample pathlength shorter than the Rayleigh range over which a Gaussian beam is focussed.

The absorption coefficient (dimensions, 1/length) is

$$\alpha(\nu) = \sum_{i,j} n_i\sigma_{ij}(\nu) \quad (2)$$

where n_i is the molecular number density in level i and $\sigma_{ij}(\nu)$ is the absorption or stimulated emission cross-section for the transition from level i to level j. In vacuum, the integrated cross-section, in SI units, is $\int\sigma_{ij}(\nu)\mathrm{d}\nu = (2\pi^2/3\epsilon_0 hc)(\boldsymbol{\mu}_{ij}\cdot\boldsymbol{\mu}_{ji})\nu_{ji}$, which is proportional to the squared magnitude of the transition dipole $\boldsymbol{\mu}_{ij}$ and to the Bohr frequency $\nu_{ji} = (E_j - E_i)/h$, where E_j and E_i are level energies,[19] h is the Planck constant, c is the speed of light in vacuum, and ϵ_0 is the permittivity of free space. Note that the proportionality to ν_{ji} implies that absorption cross-sections ($E_j > E_i$) are positive and that stimulated emission cross-sections ($E_j < E_i$) are negative. This sign convention is consistent with the sign convention for oscillator strength (positive for absorption, negative for emission)[25,26] and simplifies some formulas below. The factor of 1/3 arises from isotropic angular averaging of $\cos^2\theta$ (θ is the angle between transition dipole and optical field). Very roughly, only 1/3 of the molecules (those with transition dipoles aligned more or less parallel to the field) can effectively absorb a given polarization of light. Thus, the pump excites an anisotropic angular distribution.

At equilibrium

$$\alpha^0(\nu) = \sum_{i,j} n_i^0\sigma_{ij}(\nu) \quad (3)$$

where $\alpha^0(\nu)$ is the equilibrium absorption coefficient and n_i^0 is the equilibrium number density of level i (dimensions, 1/volume) just before pump arrival at $T = 0$. The total equilibrium molecular number density, n^0 is

$$n^0 = \sum_i n_i^0 = \sum_i n_i \quad (4)$$

where the last equality holds in the absence of photodissociation.

The spectral intensity distribution, $I(\boldsymbol{R}, \nu,)$ is related to the pulse energy $U(Z) = \int_0^\infty U(\nu, Z)\mathrm{d}\nu$ by

$$\int_{-\infty}^{+\infty}\int_{-\infty}^{+\infty} I(\boldsymbol{R}, \nu)\mathrm{d}X\mathrm{d}Y = U(\nu, Z)k_{\mathrm{rep}} \quad (5)$$

where k_{rep} is the repetition rate of the laser (pulses/time) and $U(\nu, Z)$ is the spectral energy distribution per pulse (dimensions, (energy/pulse)/frequency). The spectral energy distribution per pulse changes as the pulse propagates along Z. At each Z, the spectral energy distribution per pulse is the integral $U(\nu, Z) = \int_{-\infty}^{+\infty}\int_{-\infty}^{+\infty}u(\boldsymbol{R}, \nu)\mathrm{d}X\mathrm{d}Y$ of the energy fluence per unit frequency [dimensions, (energy/pulse)/(area·frequency)] over the transverse beam dimensions of the spatial coordinate $\boldsymbol{R}$. The energy fluence per unit frequency is written in terms of photon fluence per unit frequency, $p(\boldsymbol{R}, \nu)$ [dimensions, (photons/pulse)/(area·frequency)]

$$u(\boldsymbol{R}, \nu) = h\nu p(\boldsymbol{R}, \nu) \quad (6)$$

The pump is assumed to propagate linearly along Z, perturb level populations, and thus alter the linear propagation of the probe in the perturbed sample. The simplifying assumption of collinear pump and probe propagating along Z neglects any crossing angle between pump and probe; this neglect requires a sample pathlength short enough that spatial walk-off between the two beams can be neglected.

The total number of probe photons transmitted through the sample depends on the pump−probe delay T and the relative polarization of the pump and probe. For linearly polarized pulses, the relative polarization is quantified by $f = 3\cos^2\phi - 1$, where ϕ is the angle between pump and probe optical electric field vectors. For small beam crossing angles, the optical pathlength is negligibly longer than the sample thickness at normal incidence. The total number of transmitted probe photons (unitless) is obtained by integrating the transmitted probe fluence over frequency and the lateral beam dimensions at $Z = l$, where l is the pathlength of the sample.

$$P_r(f, T) = \int_{-\infty}^{+\infty}\int_{-\infty}^{+\infty}\left[\int_0^\infty [p_r(\boldsymbol{R}, \nu_r, f, T)|_{Z=l}]\mathrm{d}\nu_r\right]\mathrm{d}X\mathrm{d}Y \quad (7)$$

In general, anisotropic molecular excitation makes the sample dichroic and birefringent so that it can alter the polarization of the probe as it propagates (in general, fields, rather than the intensities, must be propagated). When the probe polarization is parallel or perpendicular to the pump, its polarization is not affected by propagation so that Beer's law can be used to

dx.doi.org/10.1021/jp4019662 | J. Phys. Chem. A 2013, 117, 6332−6345

describe probe propagation. With the assumptions above, the differential form of Beer's law becomes

$$\frac{\partial p_r^{on}(\boldsymbol{R}, \nu_r, f, T)}{\partial Z} = -[\alpha^0(\nu_r) + \Delta\alpha(\boldsymbol{R}, \nu_r, f, T)]\cdot p_r^{on}(\boldsymbol{R}, \nu_r, f, T) \quad (8)$$

where the superscript "on" indicates the probe field with pump excitation.

The formal solution of eq 8 is obtained by separation of variables

$$p_r^{on}(\boldsymbol{R}, \nu_r, f, T) = p_r(\boldsymbol{R}, \nu_r)|_{Z=0}\exp[-\alpha^0(\nu_r)Z]\cdot \exp\left[-\int_0^Z \Delta\alpha(\boldsymbol{R}, \nu_r, f, T)dZ'\right] \quad (9)$$

where $p_r(\boldsymbol{R},\nu_r)|_{Z=0}$ is the incident probe photon fluence at the front of the sample (which is independent of f and T and whether the pump is on or off). The integral inside the exponential is proportional to an effective change in absorbance that varies as a function of the transverse spatial coordinates X and Y; a transverse spatial variation of $\Delta\alpha$ can generate nonexponential attenuation of the spatially integrated fluence, so a spatially averaged absorbance change may not exist, but a total change in transmission ΔT remains.

Without the pump, $\Delta\alpha(\boldsymbol{R},\nu_r,f,T) = 0$, and exponential Beer's law attenuation of the probe fluence through the length of the sample is recovered:

$$p_r^{off}(\boldsymbol{R}, \nu_r) = p_r(\boldsymbol{R}, \nu_r)|_{Z=0}\exp[-\alpha^0(\nu_r)Z] \quad (10)$$

Since the excited state levels will have initially pumped populations that decay exponentially with Z due to pump attenuation, $\Delta\alpha$ will be a sum of terms that decay exponentially with Z. The appendix derives $\Delta\alpha$ by equating pump photon number depletion to initial molecular excitation, allowing for subsequent relaxation, and including transitions from excited levels, depleted levels, and levels connected by relaxation; the result obtained there is

$$\Delta\alpha(\boldsymbol{R}, \nu_r, f, T) = \sum_{i,j,k,l}\left[\int_0^\infty \Delta n_{ijkl}(\boldsymbol{R}, \nu_u, f, T)\sigma_{kl}(\nu_r)d\nu_u\right] \quad (11)$$

where $\sigma_{kl}(\nu_r)$ is the cross-section for the probe transition from level k to level l and

$$\Delta n_{ijkl}(\boldsymbol{R}, \nu_u, f, T) = \Delta n_{ijk}(\boldsymbol{R}, \nu_u, T)[1 + fr_{ijkl}(T)] \quad (12)$$

If the levels i, j, k, and l are nondegenerate, the initial anisotropy for a probe transition from level k to level l after pump excitation from level i to level j is $r_{ijkl}(T = 0) = (1/5)\cdot[3[(\boldsymbol{\mu}_{ij}\cdot\boldsymbol{\mu}_{kl})(\boldsymbol{\mu}_{lk}\cdot\boldsymbol{\mu}_{ji})/(\boldsymbol{\mu}_{ij}\cdot\boldsymbol{\mu}_{ji})(\boldsymbol{\mu}_{kl}\cdot\boldsymbol{\mu}_{lk})] - 1]$.[5] The more general theory of the anisotropy need not be a concern here as the anisotropy is simply used to relate the parallel and perpendicular pump–probe signals to level population change. At a point $\boldsymbol{R}$ in the sample, $\Delta n_{ijk}(\boldsymbol{R},\nu_u,T)$ is the total population density change in level k arising from excitation of the transition from i to j by pump frequency ν_u at a time T in the past. As shown in the appendix [eq A4], the molecular number density transferred from i to j by the pump through either absorption or stimulated emission is

$$\Delta n_{ij}(\boldsymbol{R}, \nu_u) = p_u(\boldsymbol{R}, \nu_u)|_{Z=0}n_i^0|\sigma_{ij}(\nu_u)|\exp[-\alpha^0(\nu_u)Z] \quad (13)$$

At time $T = 0$

$$\Delta n_{ijj}(\boldsymbol{R}, \nu_u, T = 0) = \Delta n_{ij}(\boldsymbol{R}, \nu_u) \quad (14a)$$

the initial change in number density in the level j is equal to the molecular number density excited, and

$$\Delta n_{iji}(\boldsymbol{R}, \nu_u, T = 0) = -\Delta n_{ij}(\boldsymbol{R}, \nu_u) \quad (14b)$$

the molecules excited to j disappear from the initial state i. If spatial migration of molecules and excitation are absent, then changes in population over time can be quantified by conditional probabilities that are independent of the spatial coordinates. Then, at later times,

$$\Delta n_{ijk}(\boldsymbol{R}, \nu_u, T) = \Delta n_{ijj}(\boldsymbol{R}, \nu_u, T = 0)c_{jk}(T) + \Delta n_{iji}(\boldsymbol{R}, \nu_u, T = 0)c_{ik}(T) \quad (15)$$

where $c_{ik}(T)$ is the conditional probability that a molecule in level i at $T = 0$ is found in level k after time T. The conditional probabilities $c_{ik}(T)$ may be calculated from chemical kinetics and will obey the initial condition $c_{ii}(T = 0) = 1$. In the absence of photodissociation, the conditional probabilities obey a sum rule, $\sum_k c_{ik}(T) = 1$, and ultimately reach thermal equilibrium, $c_{ik}(T = \infty) = g_k \exp(-\beta E_k)/q$, where g_k is the degeneracy of level k with energy E_k, β is the inverse temperature, and q is the molecular partition function.[27] With the equilibrium conditional probabilities, eqs 14 and 15 yield $\Delta n_{ijk} = 0$, and the pump–probe signal is zero.

If transitions between levels have unresolved structure, sums over sublevel relaxation kinetics can give rise to an effective cross-section for the probe transition that depends on the pump frequency and pump–probe delay (e.g., the narrowing of an electronic band upon vibrational cooling) necessitating the use of $\sigma_{kl}(\nu_r,T,\nu_u)$ in place of $\sigma_{kl}(\nu_r)$ in eq 11; then, $r_{ijkl}(T,\nu_u,\nu_r)$ may be needed in place of $r_{ijkl}(T)$ in eq 12 and $c_{ik}(T,\nu_u,\nu_r)$ in eq 15. This effective cross-section $\sigma_{kl}(\nu_r,T,\nu_u)$ will be dependent on both pump and probe frequencies until sublevel populations are thermally equilibrated. Treatment of sublevel coherence (e.g., wavepackets) via $\sigma_{kl}(\nu_r,T,\nu_u)$ is approximate, but nonequilibrium sublevel kinetics (e.g., vibrational population relaxation) can be incorporated exactly in this way.[28,29] After coherence decay and sublevel relaxation, $\sigma_{kl}(\nu_r,T,\nu_u) = \sigma_{kl}(\nu_r)$, the steady-state cross-section.

The transverse spatial profile and attenuation of the pump with depth affect the transverse spatial profile of the propagating probe intensity in eq 8. Equation 8 has the same form as Beer's law when all three of the following conditions hold: (1) the anisotropy is zero; (2) complete relaxation wipes out all correlation so that $\sigma_{kl}(\nu_r,T,\nu_u) = \sigma_{kl}(\nu_r)$; and (3) the molecules excited by the pump are spatially uniform over the probe spatial profile.

The transmitted probe photon spectrum is $\rho_r(\nu_r,f,T) = \int_{-\infty}^{\infty}\int_{-\infty}^{\infty}p_r(\boldsymbol{R},\nu_r,f,T)|_{Z=l}dXdY$, so the spectrally resolved pump–probe signal is $S_{SRPP}(\nu_r,f,T) = \rho_r^{on}(\nu_r,f,T) - \rho_r^{off}(\nu_r)$. The spectrally resolved pump–probe signal is explicitly related to $\Delta\alpha(\boldsymbol{R},\nu_r,f,T)$ using eqs 9 and 10:

$$S_{SRPP}(\nu_r, f, T) = \int_{-\infty}^{\infty}\int_{-\infty}^{\infty}p_r^{off}(\boldsymbol{R}, \nu_r)|_{Z=l}\cdot\left\{\exp\left[-\int_0^l \Delta\alpha(\boldsymbol{R}, \nu_r, f, T)dZ\right] - 1\right\}dXdY \quad (16)$$

dx.doi.org/10.1021/jp4019662 | J. Phys. Chem. A 2013, 117, 6332–6345

The pump−probe signal, $S_{PP}(f,T)$ is the change in the total transmitted probe photon number caused by the pump:

$$S_{PP}(f, T) = \int_0^\infty S_{SRPP}(\nu_r, f, T)\mathrm{d}\nu_r = \Delta P_r = P_r^{on}(f, T) - P_r^{off} \quad (17)$$

where $P_r^{on}(f,T) = \int_{-\infty}^{\infty}\int_{-\infty}^{\infty}[\int_0^\infty p_r^{on}(\boldsymbol{R},\nu_r f,T)|_{Z=l}\ \mathrm{d}\nu_r]\mathrm{d}X\mathrm{d}Y$ is the total transmitted probe photon number with the pump on and $P_r^{off}(f,T) = \int_{-\infty}^{\infty}\int_{-\infty}^{\infty}[\int_0^\infty p_r^{off}(\boldsymbol{R},\nu_r)|_{Z=l}\ \mathrm{d}\nu_r]\mathrm{d}X\mathrm{d}Y$ is the total transmitted probe photon number with the pump off.

In contrast to approaches based on the third order nonlinear susceptibility, coherent processes are formally excluded. However, correlated relaxation kinetics can be treated exactly so that some coherent processes can be incorporated approximately (e.g., the semiclassical or doorway-window descriptions of vibrational wavepackets in the integrated pump−probe signal). For comparison to experiment, the treatment here is primarily concerned with developing expressions that depend on the smallest set of independently measurable parameters. Furthermore, it automatically incorporates, to all orders, the "scheme S1/scheme S2" cascades[30] (later renamed "parallel cascades"[31,32]) necessary to describe propagation in concentrated samples when the cumulative effect of the pump over the sample length is not weak.

In the weak pump excitation regime, when the cumulative effect of the pump is also small, the exponential in eq 16 can be linearized to yield a simple expression for the spectrally resolved pump−probe signal:

$$S_{SRPP}(\nu_r, f, T) \approx \int_{-\infty}^{\infty}\int_{-\infty}^{\infty} p_r^{off}(\boldsymbol{R}, \nu_r)|_{Z=l} \cdot\left[-\int_0^l \Delta\alpha(\boldsymbol{R}, \nu_r, f, T)\mathrm{d}Z\right]\mathrm{d}X\mathrm{d}Y \quad (18)$$

This linearization requires that the integral of $\Delta\alpha$ over the propagation depth Z (proportional to an effective change in absorbance) be very much less than one. In this limit, the spectrally resolved pump−probe signal becomes proportional to a probe weighted spatial average of the transverse coordinate dependent change in absorbance or optical density. This average is often reported as $\Delta A(\nu_r)$ or $\Delta OD(\nu_r)$.[33]

Within the approximation of eq 18, if the population changes are linearly proportional to the pump pulse energy, then the signal is linearly proportional to the pump pulse energy. *However, population changes proportional to the pump pulse energy are not sufficient to guarantee that the measured pump−probe signal is linearly proportional to the pump pulse energy.* Thicker samples or higher sample concentrations require even lower excitation probabilities to suppress the cumulative higher order terms in the exponential. The quadratic term in the expansion of the exponential in eq 16 corresponds to a parallel cascade[31,32] in which the third order pump−probe signal field radiated by one molecule propagates in the same direction as the probe and then acts as the probe field in generating a pump−probe signal from a second molecule excited by the pump (hence the quadratic dependence on Δn). The mth order term involves m molecules, all m excited by the pump, but only the first interacting with the probe, in an mth order parallel cascade.

Note that the transmitted probe photon number has an implicit dependence, through Δn_{ij} in eq 13, on the pump intensity. Equations 8−10, 16, and 17 are also valid with probe intensity (I_r) and probe energy (U_r) substituted for photon fluence (p_r) and total photon number (P_r), respectively.

We now apply the above equations to the relaxation kinetics of fluorescein, simplifying to two electronic levels. The initial conditions relevant to both levels are given by eqs 14a and 14b. For the excited level j, $\Delta n_{ijj}(\boldsymbol{R},\nu_u,T) = \Delta n_{ijj}(\boldsymbol{R},\nu_u,T=0)c_{jj}(T) + \Delta n_{iji}(\boldsymbol{R},\nu_u,T=0)c_{ij}(T)$ [eq 15 with $k = j$], with $c_{jj}(T) = L_j(T)$, where $L_j(T)$ is the lifetime function of j [for a Bloch model, $L_j(T) = \exp(-T/T_1)$, where T_1 is the population lifetime]. If the levels are separated by much more than the thermal energy, the probability of a spontaneous thermal transition from i to j is zero, $c_{ij}(T) = 0$, so that

$$\Delta n_{ijj}(\boldsymbol{R}, \nu_u, T) = \Delta n_{ij}(\boldsymbol{R}, \nu_u)L_j(T) \quad (19)$$

For the ground state i, $\Delta n_{iji}(\boldsymbol{R},\nu_u,T) = \Delta n_{ijj}(\boldsymbol{R},\nu_u,T=0)c_{ji}(T) + \Delta n_{iji}(\boldsymbol{R},\nu_u,T=0)c_{ii}(T)$. Because no other state is thermally populated, $c_{ii}(T) = 1$. The conditional probability $c_{ji}(T)$ is the population of level i found by solving the relaxation equations of the system for unit population of level j at $T = 0$; it is an increasing function of T, with $c_{ji}(0) = 0$ and $c_{ji}(T = \infty) = 1$. The sum rule $\sum_i c_{ji}(T) = 1$ implies that $c_{ji}(T) \le (1 - c_{jj}(T)) = (1 - L_j(T))$; the ground state recovers population no faster than the excited state loses population. Since $c_{ji}(T) = 1 - \sum_{k\neq i}c_{jk}(T)$, setting $L_i(T) = \sum_{k\neq i}c_{jk}(T) = L_j(T) + \sum_{k\neq i,j}c_{jk}(T)$ (note the hidden dependence on j) gives $c_{ji}(T) = (1 - L_i(T))$, so that

$$\Delta n_{iji}(\boldsymbol{R}, \nu_u, T) = -\Delta n_{ij}(\boldsymbol{R}, \nu_u)L_i(T) \quad (20)$$

If only one excited level j is initially populated by the pump, then $L_i(T)$ (which depends on the initially excited state j) is the experimentally measurable ground state population recovery lifetime function. When population from the initially excited level j relaxes directly to i and subsequent thermal equilibration within i is much faster than the population relaxation from j to i, $L_i(T) \approx L_j(T)$.

The expression for the 2D spectrum obtained by leaving out the integral over ν_u in eq 11 and following the above derivation through to approximation (eq 18) agrees with previously tested expressions [eqs 17 and 18 in ref 34] for the shape of the relaxed real 2D spectrum for an electronic two level system [in the S_{2D}^- representation (eq 21 of ref 35) appropriate for a reference that passes through the sample, as in the pump−probe geometry] when the proportionalities between Einstein B coefficient line shape $g(\nu)$ and cross-section [$g(\nu) \propto \sigma(\nu)/\nu$] and between intensity and fluence [$I(\nu) \propto \nu\rho(\nu)$] are incorporated.

With a simplifying assumption that both the pump and probe pulses have no spatial chirp, the incident photon fluence in eq 6 may be written as a product of a spatial and a spectral distribution

$$p_x(\boldsymbol{R}, \nu_x)|_{Z=0} = h_x(X, Y)\rho_x(\nu_x)|_{Z=0} \quad (21)$$

where $x = u$ for pump and r for probe. With $P = \int_0^\infty \rho(\nu)|_{Z=0}\mathrm{d}\nu$, the transverse spatial distribution must be normalized so that $\int_{-\infty}^{\infty}\int_{-\infty}^{\infty}h(X, Y)\mathrm{d}X\mathrm{d}Y = 1$. Substituting in eq 21 for p_u, eq 13 becomes

$$\Delta n_{ij}(\boldsymbol{R}, \nu_u) = h_u(X, Y)\rho_u(\nu_u)|_{Z=0}\cdot n_i^0|\sigma_{ij}(\nu_u)|\exp[-\alpha^0(\nu_u)Z] \quad (22)$$

where $h_u(X,Y)$ is the spatial profile (dimensions, 1/area) and $\rho_u(\nu)|_{Z=0}$ is the frequency-dependent photon number distribution (dimensions, (photons/pulse)/frequency) of the pump at the front of the sample.

dx.doi.org/10.1021/jp4019662 | J. Phys. Chem. A 2013, 117, 6332−6345

Using labels g for ground state and e for excited state in a two-level system, the initial state is $i = g$, the pump populates $j = e$, and the probe connects level $k = e$ to $l = g$ for ESE, in addition to level $k = g$ to $l = e$ for GSB. For fluorescein at room temperature, the excited electronic state is not thermally populated and $n_e^0 = 0$. Using these labels and inserting eqs 19 and 20 into eq 12, eq 11 becomes

$$\Delta\alpha(\boldsymbol{R}, \nu_r, f, T) = \int_0^\infty \Big[+ \Delta n_{ge}(\boldsymbol{R}, \nu_u) L_e(T) \cdot [1 + fr_{geeg}(T)] \sigma_{eg}(\nu_r) - \Delta n_{ge}(\boldsymbol{R}, \nu_u) L_g(T) \cdot [1 + fr_{gege}(T)] \sigma_{ge}(\nu_r) \Big] d\nu_u \quad (23)$$

Substituting eq 22 into eq 23, eq 23 into eq 18, evaluating the integral over Z, using $\rho_r^{off}(\boldsymbol{R}, \nu_r) = h_r(X,Y)\rho_r(\nu_r)|_{Z=0} \cdot \exp[-\alpha^0(\nu_r)Z]$ (which results from inserting eq 21 into eq 10), and integrating over X and Y yields

$$S_{SRPP}(\nu_r, f, T) \approx H[P_u|_{Z=0} - P_u|_{Z=l}] \cdot \rho_r(\nu_r)|_{Z=0} \cdot \exp[-\alpha^0(\nu_r) l] \cdot \begin{bmatrix} + L_g(T)[1 + fr_{gege}(T)]\sigma_{ge}(\nu_r) \\ - L_e(T)[1 + fr_{geeg}(T)]\sigma_{eg}(\nu_r) \end{bmatrix} \quad (24)$$

where

$$H \equiv \int_{-\infty}^{+\infty} \int_{-\infty}^{+\infty} h_r(X, Y) h_u(X, Y) dX dY \quad (25)$$

is the pump−probe transverse spatial overlap, and

$$[P_u|_{Z=0} - P_u|_{Z=l}] \equiv \int_0^\infty \rho_u(\nu_u)|_{Z=0} [n_g^0 \sigma_{ge}(\nu_u)/\alpha^0(\nu_u)] \cdot [1 - \exp(-\alpha^0(\nu_u) l)] d\nu_u \quad (26)$$

is the number of pump photons absorbed by the molecules being probed. The frequency dependent fraction of photons absorbed by the molecules being probed is $[n_g^0 \sigma_{ge}(\nu_u)/\alpha^0(\nu_u)]$. For a single solute, this fraction is equal to one if the solvent does not appreciably absorb or scatter light within the pump spectrum; in this circumstance, which applies to fluorescein in methanol near 500 nm, eq 26 simply gives the total number of pump photons absorbed.

Integrating over ν_r yields the pump−probe signal in the following form:

$$S_{pp}(T, f) = H[P_u|_{Z=0} - P_u|_{Z=l}] \cdot \begin{bmatrix} + G_{ge} L_g(T)[1 + fr_{gege}(T)] \\ - G_{eg} L_e(T)[1 + fr_{geeg}(T)] \end{bmatrix} \quad (27)$$

where

$$G_{ge} \equiv \int_0^\infty \rho_r(\nu_r)|_{Z=0} \exp[-\alpha^0(\nu_r) l] \sigma_{ge}(\nu_r) d\nu_r \quad (28)$$

quantifies probe spectral overlap with the ground state bleach and

$$G_{eg} \equiv \int_0^\infty \rho_r(\nu_r)|_{Z=0} \exp[-\alpha^0(\nu_r) l] \sigma_{eg}(\nu_r) d\nu_r \quad (29)$$

quantifies probe spectral overlap with the excited state emission. (The negative sign in front of G_{eg} is the result of choosing a negative stimulated emission cross-section.)

For a two-level electronic system, the molecular parameters needed are the decadic molar extinction coefficient $\varepsilon(\lambda)$, fluorescence spectrum $F(\lambda)$, the excited state lifetime function $L_e(T)$, and the ground state bleach recovery function $L_g(T)$. Laser pulse parameters needed are the pulse spatial profile $h(X,Y)$ and pulse spectra $\rho(\nu)|_{Z=0}$. Methods for determining the required parameters are outlined in the experimental section.

EXPERIMENTAL SECTION

The goal of the experiment is 2-fold: (1) to measure the molecular and laser pulse parameters required for the calculation, and (2) to measure the absolute pump−probe signal strength for comparison against the calculation. Accurate determination of the molecular parameters required low sample concentrations and minimizing air, light, and water exposure of the organic dye solution. Measurements of concentration and sample thickness determined the decadic molar extinction coefficient $\varepsilon(\lambda)$ to ∼1% precision (with accuracy limited by mass purity). Small error bars on the pulse parameters were needed to be reasonably confident of an agreement between the measured and calculated absolute pump−probe signal strength; measurements of pump and probe spectra and spatial profiles to within 5% error were therefore necessary. The absolute pump−probe signal measurements required controlled pump−probe polarization, low pulse energies, and near-maximum spatial pump−probe beam overlap; high sample flow rates were needed to avoid pump scatter, sample photodegradation, signal saturation, and excitation of unrelaxed molecules.

A. Sample Preparation, Handling, and Integrity. Fluorescein (>97% purity, Invitrogen) was used without further purification. All fluorescein samples were prepared in 0.01 N KOH in methanol (>99.8% purity, <0.1% water) and were therefore in dianion form (pK_a = 6.8 for acid dissociation from monoanion to dianion[36]). The critical fluorescein concentration appropriate for optical experiments was established by Förster;[37] this critical concentration corresponds to the molecular separation below which energy transfer to neighboring molecules occurs within the excited state lifetime and therefore can affect pump−probe signal strength. Förster calculated the critical separation for fluorescein in 0.01 N KOH water to be ∼50 Å, corresponding to a critical concentration of ∼3 mM (for fluorescein in 0.01 N KOH methanol solution, we calculated the critical separation to be ∼51 Å). The highest concentration used in the experiment was ∼0.5 mM, ∼ 6× below the critical concentration. The decadic molar extinction coefficient, $\varepsilon(\lambda)$, was optically determined for concentrations ranging from 0.1 to 0.5 mM for two reasons: to check for aggregation, which would be concentration dependent, and to establish an accurate $\varepsilon(\lambda)$. The optical determination was done by measuring the absorbance of independently known concentrations; known masses of the dye were dissolved into known volumes of solvent (both were known to <1% error). Absorbance of the sample was measured with an absorption spectrometer (Varian Cary 500) in a 0.199 ± 0.001 mm cuvette; the manufacturer-specified path length was independently confirmed by measuring the absorbance of the same solution in a 1 cm cuvette whose path length was determined to 0.005 mm accuracy using a Starrett small hole gauge and Mitutoyo digital calipers. When the absorbance spectra were divided by cl, where c is the measured concentration and l is the sample thickness, $\varepsilon(\lambda)$s agreed within 1% error, indicating no concentration effects on $\varepsilon(\lambda)$.

dx.doi.org/10.1021/jp4019662 | J. Phys. Chem. A 2013, 117, 6332−6345

We obtained ε_{max} = 92 400 ± 90/M·cm at 497 nm for fluorescein in methanol/0.01 N KOH, which agreed within the presumed error of the previously reported literature value of 92 300/M·cm for fluorescein in ethanol/0.01 N KOH[38] (this is a lower bound on ε_{max} because of possible sample impurity; ε_{max} could be as high as 95 000/M·cm).

Preserving the sample integrity was important, as casual handling caused degradation manifested by a reduction in absorption peak height after the measurements. Light and air exposure during handling were minimized by wrapping the sample with aluminum foil and parafilm. The sample was typically used for measurements within two hours of preparation. During data collection, which typically lasted ~3−4 h, blocking the laser beams in between measurements significantly reduced degradation. The samples were prone to photodegradation caused by repeated excitation of unrelaxed sample if not refreshed after every laser shot; the sample was refreshed by rapidly flowing the sample using a Micropump (GA series) at a discharge of 2.5 mL/s through a sample cell with an 8 mm × 0.2 mm cross-section. This flow rate ensured that the average velocity for the slowest 10% of the molecules (determined by a laminar flow calculation[39] based on refs 13 and 40) was sufficiently fast that they traveled completely across the laser beam before excitation by the next pulse arriving 100 μs later (10 kHz laser repetition rate). To ensure no substantial photodegradation had occurred, absorption spectra before and after the experiments were compared. The differences were less than 4% after 3−4 h measurements when degradation was minimized as described above. In contrast, for an exposed and aged sample, up to 10% change was not uncommon.

B. Determination of Absorption and Emission Cross-Sections. The calculation ultimately demands the absorption and emission cross-sections as molecular parameters. From the decadic molar extinction coefficients, the absorption cross-section (dimension, cm^2) can be derived

$$\sigma_{abs}(\nu) = \frac{1000(cm^3/L)\cdot\ln(10)}{N_A}\varepsilon(\nu) \tag{30}$$

where $\varepsilon(\nu)$ [$=\varepsilon(\lambda = c/\nu)$] is the decadic molar extinction coefficient in 1/M·cm, and N_A is Avogadro's number in 1/mol. Here, determination of the absolute stimulated emission cross-section was based on measurement of the relative fluorescence spectrum, the absorption cross-section, the near unit fluorescence quantum yield, and the agreement between the measured fluorescence lifetime and the radiative lifetime calculated from the absorption spectrum using the Strickler−Berg relationship.[41] The accuracy of the Strickler−Berg relationship establishes the Einstein A coefficient and line shape for spontaneous emission and hence the Einstein B coefficient and line shape for stimulated emission (needed to calculate the absolute stimulated emission cross-section). As the Strickler−Berg relationship depends on the Condon approximation, this integrated agreement between the calculated and measured fluorescence lifetimes supports the average validity of the Condon approximation for this electronic transition in fluorescein. The relative fluorescence spectrum [$F(\lambda)$ in photon counts/(s·nm)] was recorded using 470 nm excitation on a Fluorog (Horiba Jobin-Yvon) fluorimeter calibrated for vacuum wavelength. The area normalized line shape function for the stimulated emission Einstein B coefficient was derived from the fluorescence line shape using the relationships $\lambda = c/\nu$ and

$$g_{em}(\nu) = [F(\lambda = c/\nu)/\nu^5]/\int_0^\infty [F(\lambda = c/\nu)/\nu^5]d\nu \tag{31}$$

where $1/\nu^5 = (1/\nu^2) \times (1/\nu^3)$, with $1/\nu^2$ proportional to the Jacobian in going from even wavelength intervals to even frequency intervals ($\delta\lambda \rightarrow \delta\nu$) and $1/\nu^3$ proportional to the factor relating Einstein A (spontaneous emission) and B (stimulated emission) coefficients.[42] The absolute stimulated emission cross-section was obtained from the normalized emission line shape function $g_{em}(\nu)$ by using the relationship

$$|\sigma_{eg}(\nu)| \equiv \frac{h\nu}{c}B_{eg}g_{em}(\nu) \simeq \frac{h\nu}{c}B_{ge}g_{em}(\nu) \equiv \nu g_{em}(\nu)\int_0^\infty \frac{\sigma_{ge}(\nu')}{\nu'}d\nu' \tag{32}$$

where $\sigma_{ge}(\nu')$ is the frequency-dependent absorption cross-section and the prime denotes a dummy frequency variable. Division and multiplication by ν inside and outside the integral on the last line arises from the relationship between B and σ on the first line, which also holds for the absorption cross-section, $\sigma_{ge}(\nu) = (h\nu/c)B_{ge}g_{abs}(\nu)$.[19] The approximation in eq 32 arises because the change in equilibrium geometry between ground and excited state may allow $B_{ge} \neq B_{eg}$ for relaxed spectra; it is exact if the Condon approximation holds over the full range of both ground and excited state equilibrium coordinate distributions. The agreement between the experimental literature lifetime (4.28 ns)[43] and that calculated from the Strickler−Berg relationship (3.97 ns) was within 10% error, suggesting the Condon approximation is valid on average.

Figure 1 shows the S_0−S_1 absorption and emission cross sections as a function of frequency. The emission cross section roughly mirrors the absorption cross section. The obvious difference in the maximum cross-section reflects both the wider normalized emission line shape (~20% wider than the absorption line shape) and the proportionality of cross-section to frequency. In Figure 1, the laser pulse spectrum is overlaid to

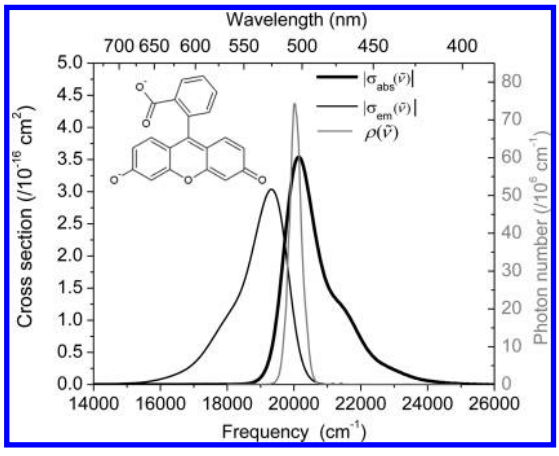

Figure 1. Optically determined S_0−S_1 cross sections for absorption, $\sigma_{ge}(\tilde{\nu})$ (thick solid line), and emission, $|\sigma_{eg}(\tilde{\nu})|$ (thin solid line), of fluorescein in methanol/KOH (~0.01 N). The absolute pump pulse laser spectrum $\rho(\tilde{\nu})$ is overlaid (vertical axis at right). The laser pulse parameters are pulse energy, U = 13.5 ± 0.80 nJ; maximum pulse intensity at $\tilde{\nu}_{max}$ = 20 023 cm^{-1} (499.4 nm λ_{max}); width of the pulse spectrum $\Delta\tilde{\nu}_{fwhm}$ = 430 ± 26 cm^{-1} (10.7 nm $\Delta\lambda_{fwhm}$). The inset shows the molecular structure of fluorescein dianion.

dx.doi.org/10.1021/jp4019662 | J. Phys. Chem. A 2013, 117, 6332−6345

give an idea of how it overlaps with the cross-sections; the pump−probe signal calculation essentially involved the overlap of the pulse spectra and cross-section.

C. Pump−Probe Experiment Setup. The schematics of the femtosecond laser setup employed for the pump−probe experiment are shown in Figure 2. The femtosecond pulses

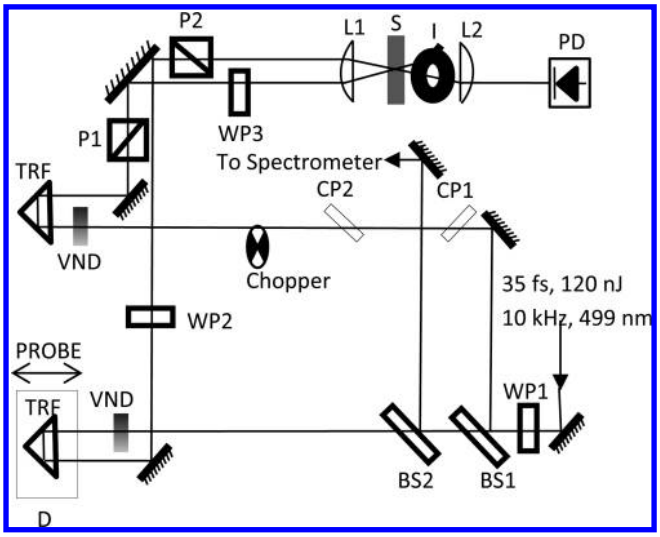

Figure 2. Femtosecond pump−probe experiment. WP1, WP2, and WP3, zero order half waveplates; BS1 and BS2, 50:50 fused silica femtosecond laser beamsplitter for *p*-polarized light; CP1 and CP2, antireflection coated fused silica compensating plates; TRF, trihedral retroreflector; P1 and P2, calcite cube polarizers; L1 and L2, $f = 10$ cm plano-convex focusing lenses; S, sample flowcell; I, iris; PD, Si photodiode detector; VND, variable neutral density filter; D, translation stage for pump−probe time delay.

were generated from a home-built noncollinear optical parametric amplifier (NOPA),[44,45] pumped by an 80 fs, 800 nm, 7 μJ regenerative amplifier running at 10 kHz repetition rate (Coherent RegA 9050). The NOPA delivered horizontally polarized pulses having up to 200 nJ energy, tunable from 480 to 750 nm. NOPA pulses typically had ∼400 cm^{-1} full width half-maximum (fwhm), easily compressible below 40 fs using a pair of fused-silica prisms. The spectrum was shaped to nearly Gaussian by means of razor blades placed after the second compressor prism.

The polarization of the beam before splitting it to a strong pump and weak probe was rotated to vertical, using an achromatic zero-order quartz-MgF_2 $\lambda/2$ wave plate [0.52 retardance at 500 nm (Newport 10RP52-1)]. After the beamsplitter (CVI Melles-Griot, FABS-550-45P-PW-1006-UV − this 50:50 beamsplitter designed for p-polarized femtosecond pulses at 550 nm wavelength generates unequal pulse energies for s-polarized pulses at 500 nm wavelength), the pump and probe beams traveled separate beam paths; the probe beam path length was variable via a computer controlled (Newport MM3000) mechanical translation stage (Newport MTM200PP.1) for up to 20 cm, allowing a pump−probe delay up to ∼1 ns. The dispersions in both beams were matched using identical uncoated air-spaced glan prism calcite polarizers (Karl Lambrecht, MGTYE8, 5×10^{-6} extinction), metallic variable neutral density filters (Edmund Optics), and zero-order $\lambda/2$ waveplates (Newport 10RP52-1). The energies of the pump and probe beams were independently varied using the variable neutral density filters. For polarization-dependent pump−probe measurements, the pump polarization was varied using the pump zero-order $\lambda/2$ waveplate; the waveplate was placed after the last mirror before the sample to preserve the pump polarization, which can be scrambled if reflection off a mirror is neither *s* nor *p*. The probe polarizer was placed after the last mirror before the sample to make sure the probe polarization was vertical. The pump and probe polarizations were checked by using an analyzer polarizer placed behind the sample after the collimating lens to measure the extinction ratios. The extinction ratio was 121:1 when setting the pump or probe polarization to either parallel or perpendicular and rotating the analyzer to give either maximum or minimum transmission.

The pump and probe beams were focused into the sample by a 10 cm focal length BK7 glass lens, coated to prevent reflective loss in the visible range. The pump and probe beams were overlapped at the focus by maximizing their transmission through a 50 μm pinhole. The pump and probe beams were separated by 1.2 cm on the 10 cm focal length lens. At 500 nm wavelength, the beam crossing angle becomes 5° in the methanol sample, so the optical pathlength is a negligible 0.1% larger than the sample thickness. The interferometer alignment was checked by monitoring probe transmission through the pinhole over a 1 ns time delay; the transmitted probe energy varied less than 2%, indicating a good alignment over the entire probe delay range.

Once a good spatial overlap was found, the zero pump−probe delay was found by autocorrelation with 100 μm thick KDP cut at 40°, which also allowed pulse duration measurements. After further optimization of dispersion compensation by changing the tip to tip prism distance and amount of prism insertion into the beam, ∼38 fs pulse duration was obtained for a beam centered at 500 nm with ∼12 nm fwhm (34 fs transform limited pulse duration). After crossing the pump and probe beams in the sample, the transmitted probe energy was measured by a silicon PIN photodiode with an active area of 4.6 mm diameter and a rise time of 30 ns (Electro-Optics Technology ET2040) (the pump beam was blocked by an iris as soon as it exited the sample). To reduce the scattered beams reaching the probe photodiode, several irises were placed along the probe path from sample to photodiode, the photodiode was placed in a blackened box, and stray lights were blocked at their sources.

For pump−probe transients (the change in transmitted probe photon number as a function of pump−probe delay) lock-in detection was used. The 500 Hz modulated probe signal from the photodiode was sent to a digital lock-in amplifier (Stanford Research SR830) referenced at the pump chopping frequency. The pump-induced change in transmitted probe photon number was detected by the lock-in amplifier and sent to the A/D converter (Stanford Research SR245). The lock-in time constant was set at 10 ms, which was sufficient for smoothing fast fluctuating noise, mainly coming from particle scatter in the sample (no liquid filters were used in the sample flow system because they can collect molecules, changing the concentration). The sample cell was translated along the focus to maximize the pump-probe signal for 0.2 mM fluorescein, and fixed there for all measurements. Over the 0.2 mm sample pathlength, beams overlapped in the middle of the sample cell walk off by 9 μm at each end. For the 43 μm beam diameter, (see below) this reduces the pump-probe spatial overlap integral *H*, averaged over the sample cell length, by 2%, justifying neglect of spatial walk-off.

dx.doi.org/10.1021/jp4019662 | J. Phys. Chem. A 2013, 117, 6332−6345

For fixed delay absolute signal strength measurements, the absolute voltages generated by the probe photodiode with the pump on (V_{on}) and off (V_{off}) were measured using a gated integrator (boxcar). Multiple sequences of pump-on and -off voltages were recorded by chopping the pump beam at 4 Hz. The output of the probe diode was amplified 5× by a Stanford Research SR445A preamplifier and sent to a gated integrator and boxcar (Stanford Research ~~SR245~~). The boxcar was triggered by the laser amplifier signal from the RegA electronics. The boxcar integrated the photodiode output for each pulse over a 100 ns gate, and the last sample output was read by a 13-bit resolution analog-to-digital converter through a GPIB interface. Measurement data files generated using the boxcar measurements were analyzed by a software algorithm to extract average V_{on} and V_{off}. The difference in voltages $\Delta V = V_{on} - V_{off}$, divided by the voltage with the pump off (V_{off}), was equal to $\Delta P_r/P_r^{off}$ where P_r^{off} was the transmitted probe photon number with the pump off and ΔP_r is the change in transmitted probe photon number caused by the pump [the pump − probe signal we are interested in, see eq 17]. For both pump and probe, incident and transmitted photon numbers were determined with a power meter [Coherent FieldMaster GS display (1% accuracy) and LM-2Vis sensor (5% accuracy)] to within 6% error; thus, ΔP_r was determined with better than 6% error from the voltage measurements.

D. Determination of the Laser Spatial Profile and Spectra. The femtosecond pulses were characterized to determine their spatial and spectral profiles. The spatial profile was determined by imaging the focused beam on a CMOS based color web camera with its lens removed (ZoomCam 1598, 640 × 480 resolution; we were unable to obtain a pixel size specification). By imaging a 1.00 ± 0.025 mm grid pattern (National Brand, engineering form graph paper # 12-188) attached to the surface of the CMOS censor, the average pixel spacing was determined in both dimensions to be 7.35 μm/pixel. The beam images were corrected for saturation using the measured detector saturation function vs beam intensity. For the beam focused with 20 cm lens, the spatial profile fitted a 2D Gaussian of the form $h(X,Y) = A \exp[-\{(X^2/w_X^2) + (Y^2/w_Y^2)\}]$, where A is a constant, X and Y are the Cartesian coordinate distances from beam center and $w_{X,Y}$ the $1/e$ half widths along two orthogonal axes (not necessarily aligned with the CMOS array axes). The 2D profile was nearly circular with w_X/w_Y ratio ≈ 0.9. The resolution of the camera was inadequate to image the beam focused by the 10 cm lens. For the beam focused with the 10 cm lens, the beam diameter (defined as that of the circular aperture giving 50% transmission) was determined by energy transmission through 25, 50, and 75 μm diameter pinholes. The diameters estimated with different pinhole sizes all agreed within 6% of 43 μm. This diameter was within 4% of the diffraction limited focal spot size for a Gaussian beam. The Rayleigh range, over which focused Gaussian beams increase by $2^{1/2}$ in size,[46] is 8 mm, justifying the approximation of collimated Gaussian beams[24] for the 0.2 mm sample pathlength.

The pulse spectra as a function of wavelength were determined using a grating spectrometer with a linear silicon CCD array detector (Ocean Optics, USB4000 UV−vis). The beam was diffused by passing through a few layers of tissue and guided into the spectrometer via multimode optical fiber (Ocean Optics P300-1-SR). The spectrometer measured photons per unit wavelength. The calibrated pulse spectra corresponding to photons per unit frequency [$\rho(\nu)$], were obtained by (1) multiplying the corresponding frequency scale spectra by $1/\nu^2$, the Jacobian in going from wavelength to frequency intervals; (2) area normalizing the frequency spectra from step 1; and (3) multiplying the area normalized frequency spectrum by the total number of photons in the pulse $U/h\nu_{500nm}$ [where U is the pulse energy determined with the silicon photodiode power meter (Coherent FieldMaster LM-2Vis), set on the energy calibration for 500 nm, by measuring average power and dividing by the laser repetition rate]. The pump and probe spectra were identical within <0.1% error and were fitted to a Gaussian of the form $\rho'(\tilde{\nu}) = \rho_{max} \exp[-(\tilde{\nu} - \tilde{\nu}_0)^2/\Delta^2]$, where ρ_{max} is the maximum number of photons per unit frequency interval, $\tilde{\nu}_0$ is the frequency maximum in cm^{-1}, and Δ is half the $1/e$ width (= fwhm/(2(ln(2))$^{1/2}$) in cm^{-1} (the prime serves to denote ρ' as a fit function that differs from the actual spectrum). Area normalizing the Gaussian, $\rho_{max} = U/(h\nu_{500nm}(\Delta^2\pi)^{1/2})$. From the fit, $\tilde{\nu}_0$ = 19 991 ± 2 cm^{-1} and Δ= 257 ± 0.5 cm^{-1}. [Although determined from the same spectrum, $\tilde{\nu}_0 \neq \tilde{\nu}_{max}$ and $\Delta \neq 2(\ln(2))^{1/2}\Delta\tilde{\nu}_{fwhm}$ in Figure 1 because $\tilde{\nu}_{max}$ and $\Delta\tilde{\nu}_{fwhm}$ are determined directly from $\rho(\tilde{\nu})$; similarly, λ_{max} and $\Delta\lambda_{fwhm}$ are determined from $\rho(\lambda)$, so $\tilde{\nu}_{max} \neq 1/\lambda_{max}$ because the wavelength interval contained in a constant frequency interval depends on wavelength (as reflected in the Jacobian).] The frequency-dependent photon distribution function in terms of the pulse energy, center frequency, and the width is $\rho'(\tilde{\nu}) = U/(h\nu_{500nm}(\Delta^2\pi)^{1/2}) \exp[-(\tilde{\nu} - \tilde{\nu}_0)^2/\Delta^2]$. Stable operation of the femtosecond laser (typically, the pulse to pulse energy fluctuation was ∼1%) was critical to maintaining uniform spatial and spectral pulse profiles over the course of measurements and was, in turn, necessary to achieve a good signal-to-noise ratio.

E. Beer's Law Check. Beer's law requires linear pulse propagation that is explicitly assumed in the calculation. Energetic femtosecond pulses that generate very high peak powers with low average powers can cause a breakdown of Beer's law.[20] Sufficiently weak femtosecond pulses may propagate linearly, with attenuation governed by Beer's law (and phase shift governed by the refractive index).[46] To check that Beer's law was obeyed for the femtosecond laser pulses used in the experiments, we measured the transmitted pulse energy as a function of incident pulse energy and compared the measurements to calculations using the laser pulse spectrum and absorption spectrum. The measured fraction of photons absorbed, 0.94 ± 0.02, matched well with the calculated fraction of 0.93 ± 0.01 using the following independently measured experimental parameters: 0.81 mM fluorescein in a 0.200 mm thick flow cell (peak absorbance of 1.28 at 496 nm); 0.3 to 13.5 nJ incident laser pulse energy (0.2% to 8.8% excitation probability when averaged over the 43 μm diameter Gaussian beam and the 0.2 mm sample path length); $\tilde{\nu}_{max}$ = 20 023 cm^{-1}; $\Delta\tilde{\nu}_{fhwm}$ = 430 cm^{-1}; 38 fs pulse duration. Reflective losses from the front and back surfaces (∼8% in total) were accounted for by measuring transmitted power through the flow cell with a methanol blank solution.

F. Pump−Probe Signal Linearity Check. The linearity of the pump−probe signal with respect to the pump pulse energy was checked by power dependence measurements at two fixed pump−probe delays; one at T = 100 fs when the pulse overlap was over and one at T = 100 ps when all vibrational coherence had decayed. The experimental parameters were 0.298 ± 0.004 mM fluorescein in a 0.20 mm thick flow cell; $\tilde{\nu}_{max}$ = 20 023 cm^{-1}; $\Delta\tilde{\nu}_{fhwm}$ = 430 cm^{-1}; 38 fs pulse duration. The pump pulse energy was varied from 1 to 8 nJ in 0.5 nJ steps; the

dx.doi.org/10.1021/jp4019662 | J. Phys. Chem. A 2013, 117, 6332−6345

weighted average of the excitation probability ranged from 1% to 8.9%. After carefully establishing the zero signal level, the pump−probe signal vs pulse energy fitted a linear function $S = cU_u + d$, where c is a proportionality constant, U_u is the pump pulse energy, and d is an arbitrary constant, with reduced χ^2 = 1.16. The fit parameters were c = 0.0510 ± 0.0004 (at 100 fs) and 0.0384 ± 0.0002 (at 100 ps) and d = −0.02 ± 0.02 (at 100 fs) and −0.014 ± 0.015 (at 100 ps) for signals S ranging from 0 to 0.2. Since intercepts were poorly determined (errors are bigger than the intercepts), the fit constrained them to zero, which did not significantly increase the reduced χ^2. A quadratic coefficient also did not improve the fit and was zero within error. The slopes are determined to within 1% error, indicating near perfect linearity for pump pulse energies varying nearly 1 order of magnitude.

RESULTS

First, the pump−probe measurements as a function of pump−probe delay at parallel, perpendicular, and magic angle pump−probe polarizations are presented. The time dependent kinetics is described and compared to the literature. Next, we show the calculation compared to measurements. Two calculations are discussed; one for the time dependence of the pump−probe signal with magic angle polarization and another for the concentration dependence of the pump−probe signals at a fixed pump−probe delay (long after vibrational and rotational coherences have decayed).

A. Pump−Probe Transients. Figure 3 shows the time-dependent pump−probe signals measured at parallel, perpendicular, and magic angle polarization. Overlaid is the magic angle signal reconstructed from the parallel and perpendicular signals and fits. The parallel, perpendicular, and magic angle

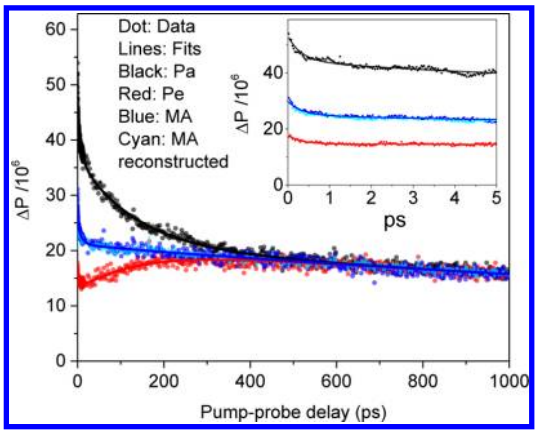

Figure 3. Measured absolute fluorescein pump−probe signal as a function of pump−probe delay for parallel (black), perpendicular (red), and magic angle (blue) pump−probe polarization. The vertical axis is the change in transmitted probe photon number. The magic angle signal constructed from the parallel and perpendicular signal $MA = (PA + 2PE)/3$ is overlaid (cyan). Inset: Same plot for the first 5 ps. Fluorescein concentration in 0.01 N KOH methanol, 0.298 ± 0.004 mM; pump pulse energy U_u = 3.12 ± 0.19 nJ; probe pulse energy U_r = 0.506 ± 0.03 nJ; beam diameter 43.5 ± 2.6 μm (50% transmission through a 43.5 μm diameter pinhole); maximum pulse intensity at $\tilde{\nu}_{max}$ = 20 023 cm^{-1}; width of pulse spectrum $\Delta\tilde{\nu}_{fwhm}$ = 430 ± 26 cm^{-1}; 38 fs pulse duration. The probe transmission with the pump off was 0.33 ± 0.02. The total incident probe photon number was (1.27 ± 0.08) × 10^9.

pump−probe signals were globally fitted to a model function based on eq 33:

$$S_{pp}(f, T) = S_{iso}(T)[1 + fr(T)] \quad (33)$$

where $S_{iso}(T)$ described the isotropic dynamics (ideally, the magic angle signal), $r(T)$ is the time-dependent anisotropy, and the index f quantifies the relative angle between pump and probe polarization [f is defined between eqs 6 and 7; f = 2 for parallel, 0 for magic angle, and −1 for perpendicular]. The isotropic dynamics is modeled by a sum of three exponentials [eq 34]

$$S_{iso}(T) = A_1\exp(-T/\tau_1) + A_2\exp(-T/\tau_2) + A_3\exp(-T/\tau_3) \quad (34)$$

with two exponentials describing dynamics faster than 20 ps and one exponential describing nanosecond dynamics. The anisotropy is modeled by a sum of a Gaussian and an exponential [eq 35]

$$r(T) = A_G\exp[-(T/\tau_G)^2] + A_{aniso}\exp(-T/\tau_{aniso}) \quad (35)$$

with the Gaussian describing inertial rotational dynamics[47] and the single exponential describing rotational diffusion.[5] The results of the global fit are summarized in Table 1. The 331 ± 22 fs component, which accounts for ∼17% of the total amplitude, coincides reasonably with methanol polar solvation; literature time scales are 280[48] and 340 fs.[42] The 9.54 ± 0.33 ps component with ∼13% of the total amplitude is roughly intermediate between the two components at 3.20 and 15.3 ps that Horng et al.[48] report in studies of methanol solvation dynamics using a coumarin dye (fluorescein contains much of the coumarin structure); the two components have amplitudes approximately equal to each other in their study. It is possible that the fitting routine used here assigned a single averaged component that might separate into two with higher signal-to-noise. Vibrational relaxation may also occur on 10−100 ps time scales. We attribute the 3.58 ± 0.33 ns component, which accounts for ∼70% of the total amplitude, to the fluorescein fluorescence lifetime. This time constant is ∼17% smaller than the literature value (4.28 ± 0.07 ns),[43] but the measurement here had a 1 ns maximum pump−probe delay and so is unlikely to accurately capture a ∼4 ns lifetime. A shorter lifetime could also arise from fluorescence quenching (for example, by dissolved oxygen[49]) in the measurements reported here. The 137 ± 1.5 ps anisotropy decay component is in good agreement with the 140 ps literature value.[50] The experimental initial anisotropy, $r(0)$ = 0.396 ± 0.003 is close to the expected value of 2/5; this agreement suggests that saturation (which reduces the initial anisotropy in pump−probe experiments[13]) is negligible (the statistical error bar does not account for systematic error from the polarization extinction ratio of 121:1). The Gaussian inertial component was necessary to accurately capture the first 2 ps data; without it, there was a systematic under-estimation in the fit. The 2.7 ± 0.5 ps inertial component, which accounts for ∼4% of the total anisotropy decay amplitude, is longer than that reported in the ultrafast dichroism study of anthracene (∼400 fs).[47] Although the Gaussian component alleviated the misfit in the first 2 ps of the anisotropy, the signal-to-noise ratio may not be sufficient to pin down the time scale.

B. Comparison to Calculation. Figure 4 shows the calculated [using eq 27] and measured time-dependent pump−probe signal at magic angle pump−probe polarization. The

dx.doi.org/10.1021/jp4019662 | J. Phys. Chem. A 2013, 117, 6332−6345

Table 1. Global Fit Parameters for Fluorescein Dianion in Basic Methanol Recovered from Parallel, Perpendicular, and Magic Angle Pump−Probe Experiments[a]

A_1	τ_1 (fs)	A_2	τ_2 (ps)	A_3	τ_3 (ns)
0.209 ± 0.008	331 ± 22	0.157 ± 0.003	9.54 ± 0.33	0.881 ± 0.002*	3.58 ± 0.04*
A_G		τ_G (ps)	A_{aniso}		τ_{aniso} (ps)
0.017 ± 0.002		2.70 ± 0.47	0.383 ± 0.001		137 ± 1.5

[a]The fit function was $[A_1 \exp(-t/\tau_1) + A_2 \exp(-t/\tau_2) + A_3 \exp(-t/\tau_3)]\cdot[1+f\{A_G \exp[-(t/\tau_G)^2] + A_{aniso} \exp(-t/\tau_{aniso})\}]$. f was set at 2 for parallel and −1 for perpendicular but was allowed to float for magic angle (the best fit value was $f = 0.04$ when ideally $f = 0$; the best fit f corresponds to a polarizer set at 53.9°, a 0.8° deviation from the 54.7° magic angle). The nominal 1σ error bars correspond to a unit increase in χ^2. *The error bars for A_3 and τ_3 increase to ±0.07 and ±0.33 ns, respectively, when an overall signal offset is allowed to float within the ±0.003 uncertainty of the zero baseline established for signal at negative T.

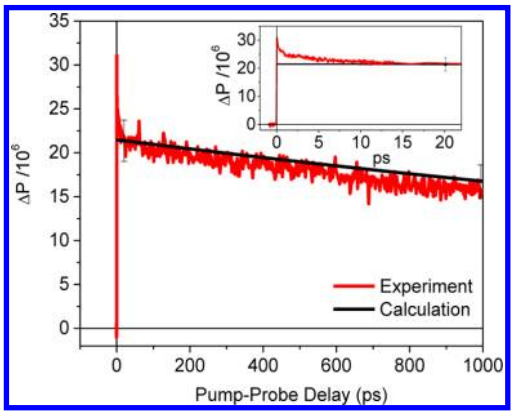

Figure 4. Magic angle change in transmitted probe photon number as a function of pump−probe delay. Inset: The same plot for the first 20 ps. The experimental measurement (red) is compared to a calculation without any adjustable parameters (black). The error in the calculation is indicated assuming ±6% variation in the beam diameter, ± 6% variation in the pump and probe pulse energies. Fluorescein concentration in 0.01 N KOH methanol, 0.298 ± 0.004 mM; pump pulse energy U_u = 3.12 ± 0.19 nJ; probe pulse energy U_r = 0.506 ± 0.03 nJ; beam diameter 43.5 ± 2.6 μm (50% transmission through a 43.5 μm diameter pinhole); maximum pulse intensity at $\tilde{\nu}_{max}$ = 20 023 cm^{-1}; width of the pulse spectrum $\Delta\tilde{\nu}_{fwhm}$ = 430 ± 26 cm^{-1}; pulse duration 38 fs. The probe transmission with the pump off was 0.33 ± 0.02. The total incident probe photon number was (1.27 ± 0.08) × 10^9.

calculation agreed with experiment within 10% error. The spatial profiles were modeled by a circular 2D Gaussian; $h'(X,Y) = 1/(w^2\pi) \exp[-(X^2 + Y^2)/w^2]$ (the prime is to denote it is a fit function) where $(X^2 + Y^2)^{1/2}$ is the radius and w is the $1/e$ half width (the 50% transmission beam diameter is $2w(\ln(2))^{1/2}$). Assuming the pump and probe beam to be identical and have perfect spatial overlap (these assumptions were justified by the measurements), $H = 1/(2w^2\pi)$. In general, H can be evaluated numerically without any assumption using the measured $h(X,Y)$. The pump pulse spectra $\rho_u(\nu_u)$ and probe pulse spectra $\rho_r(\nu_r)$ at the sample spot were obtained by the method detailed in the experimental section. Raw spectra (not the Gaussian fit) were used in the calculation. However, the previously defined fit functions $h'(X,Y)$ and $\rho'(\tilde{\nu})$ were useful because the relationship between the pulse parameters and the strength of the pump−probe signal was explicitly revealed; assuming spatially and spectrally identical pump and probe pulses, the pump−probe signal is proportional to the factors, $(1/2w^2\pi)\cdot(1/\Delta^2\pi)$ where w is half the $1/e$ beam diameter and Δ is half the $1/e$ spectral width (the first factor arises from the normalization constant for the spatial Gaussian fit function, and the second factor is the square of the normalization constant for the spectral Gaussian fit function). The polarization index f was set to 0 for magic angle pump−probe polarization. The parallel and perpendicular signals were calculated using the literature[50] anisotropy function $r(T)$, which was assumed to be the same for the excited and ground state. The calculation agreed with measurements within ∼10% error (see Figure 4). The time-dependent dynamics was solely dictated by the lifetime function for which the lifetime constant was set to the literature result, 4.28 ± 0.07 ns.[43] The inset in Figure 4 shows the first 20 ps of the same plot. The calculation deviated from the measurement by more than 10% for pump−probe delay below 20 ps. This discrepancy was expected from the fit results of the experimental data that showed a few hundreds of femtoseconds to picoseconds dynamics; the calculations did not include solvation or vibrational wavepacket dynamics [which can be incorporated through correlation in the cross-section $\sigma(\nu_r,T,\nu_u)$]. This comparison established that, for delays of less than ∼20 ps, the approach taken to calculate the pump−probe signal is inadequate, and a treatment based on the third order nonlinear susceptibility or response function is needed.

Figure 5 shows the calculated and measured concentration-dependent pump−probe signals with the parallel pump−probe polarization at 600 ps pump−probe delay. The rotational relaxation was over by 600 ps so the signals were independent of pump−probe polarization; the signals from all three polarizations converged to the same value within 3% error for 0.20 and 0.56 mM concentrations. The measured signals fell within ∼10% of the calculation for the range of concentrations measured (from 0.03 to 0.56 mM). This concentration range contains both the rise and fall of the signal around its maximum.

DISCUSSION

The good agreement between the calculations and measurements demonstrates that the required set of theoretical assumptions and experimental conditions are sufficiently met for fluorescein. All calculated population changes in the ground and excited states are accounted for by the measurement within error. Experimental requirements for this agreement are uniform pump-probe spatial overlap throughout the sample, determination of the beam diameter and spectrum width to within 5%, and keeping the laser noise to less than 1% in order to keep the error in the calculation less than ∼10%; the good agreement allows for quantitative physical interpretation (see below). $\varepsilon(\lambda)$ and $F(\lambda)$ can be determined with better than 1% precision but are prone to systematic errors with too high concentration or poorly determined sample path length; we have observed distortion of the absorption shape at $OD \approx 1.5$ and the peak of Figure 5 shift by 10% for 7.5% error in the

dx.doi.org/10.1021/jp4019662 | J. Phys. Chem. A 2013, 117, 6332−6345

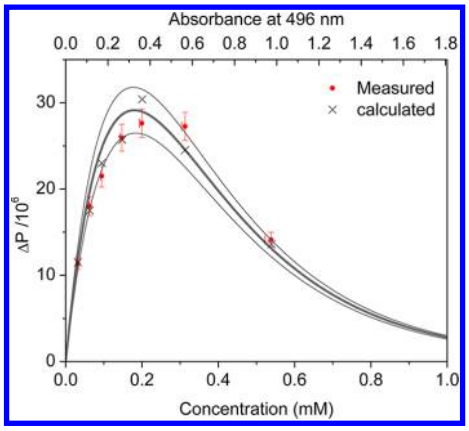

Figure 5. Measured (solid circle) and calculated (× and line) pump−probe signals as a function of concentration. Discrete calculations (× and error bars) used the experimental parameters of the individual measured signals. The thick continuous line is a calculation using the average pump and probe pulse energies for the entire series of measurements. Thin gray lines indicate calculated upper and lower bounds on the calculated signals using the average pulse energies for the series. Vertical bars just to the left of data points indicate lower bounds on concentration. Parallel polarization; pump−probe delay T = 600 ps; pump pulse energy U_u ranged from 4.55 to 4.61 nJ with ∼6% systematic error; probe pulse energy U_r ranged from 0.464 to 0.480 nJ with ∼6% systematic error; beam diameter 43.5 ± 2.6 μm (50% transmission through a 43.5 μm diameter pinhole); maximum pulse intensity at $\tilde{\nu}_{max}$ = 20 023 cm^{-1}; width of the pulse spectrum $\Delta\tilde{\nu}_{fwhm}$ = 430 ± 26 cm^{-1}; 38 fs pulse duration.

sample length. Checks for linear pulse propagation and linear pump pulse energy dependence of the pump−probe signal are important to establish that data are free of high order effects that are not included in the theoretical treatment; in our experiments, measurements confirmed the pulse propagation and signal linearity. In femtosecond measurements, low excitation probabilities are necessary. However, for thick samples or higher concentrations, even lower excitation probabilities may be required to ensure linearity against cascades. The calculation of excitation probabilities as a function of the sample depth for the pulses used in the experiments shows that the local excitation probability is a steeply varying function of depth; for C = 0.298 mM, U_u = 3.12 nJ, and w = 26.1 μm (50% transmission through a 43.5 μm diameter pinhole), the local excitation probabilities in the center of the Gaussian beam where the energy is highest were ∼12% at the front and ∼4% at the back of the sample, although the average excitation probability over the sample depth and transverse profile is ∼6%. With a polarized beam, for molecules aligned parallel to the laser polarization, the excitation probability is three times higher (36% in the worst case scenario at sample front and beam center). Thicker samples or higher sample concentrations run the risk of cumulative effects that manifest as a parallel cascade; this effect corresponds to the quadratic and higher order terms in the expansion of the outer exponential of eq 16, which are neglected in eq 18. Experimentally significant cumulative effects are not detected in this data; the calculations suggest that quadratic terms contribute less than 3% to the total signal.

The calculation and measurement are not simple, and their agreement for fluorescein suggests that both are correct within the limits stated. In experiments carried out before the fluorescein measurements, measurement and calculation did not agree for three structurally related tricarbocyanine dyes (IR144, IR125, and HDITCP), even though they are well-known to behave as electronic two-level systems near 800 nm,[51] and the dynamics on femtosecond and picosecond time scales have been attributed to solvation and vibrational relaxation in several studies.[42,52−54] The preliminary measurements of the absolute pump−probe signal on these tricarbocyanines are consistent with relaxation channels that drain up to half of the excited state population within a few hundred femtoseconds. Mechanisms for fast population relaxation have been described for smaller symmetrical cyanines.[55−57] The presence of fast population decay channels may partially explain why the reported 2% fluorescence quantum yield for IR 144 in methanol[58] is significantly lower than the ∼8% quantum yield that would be deduced from the slowest exponential decay of 445 ps (previously interpreted as the lifetime)[42,58] and the radiative lifetime of ∼5.8 ns that we calculate from the Strickler−Berg relationship.[41] Evidently, some of the femtosecond and picosecond signal decay previously attributed to solvation of these tricarbocyanines arises from vibrational or solvent coordinate dependent ultrafast excited state population decay, and their nonexponential lifetime function $L_e(T)$ must be determined by comparing calculated and measured absolute pump−probe signal strengths. To enable a test without unknown parameters, fluorescein was chosen for subsequent experiments because the fluorescence quantum yield is almost one,[38,43] the emission lifetime obeys the Strickler−Berg relationship,[41] and the absorption spectrum of the first excited singlet state[59] does not overlap the pulse spectra. The pump−probe method demonstrated here may also determine the excited state absorption cross-section if the lifetime function is known.

While the agreement in fluorescein is good for pump−probe delays greater than 20 ps, matching the measured and calculated signals at earlier times requires either the extension to time-dependent cross-sections [2D spectroscopy seems to naturally measure the products $\sigma_{ji}(\nu_u)c_{ik}(T,\nu_u,\nu_r)\sigma_{kl}(\nu_r,T,\nu_u)$] or, more generally, use of the third order nonlinear susceptibilities. The approach presented here can anchor the absolute signal for these more general approaches at large pump−probe delays. Meanwhile, the current approach can be improved in at least 3 ways: (1) an absolute radiative rate can be used to determine the emission cross-section[60] removing the need for the Condon approximation;[61] (2) the measured pump−probe signal can be spectrally dispersed to obtain transient spectra that are calibrated in absolute photon number (combined with global analysis, this may be sufficient for many multilevel systems); and (3) the two beam pump−probe experiment for measuring the spectrally resolved pump−probe transients can be converted to a "HARD 2D"[62] experiment to obtain 2D spectra with amplitude calibrated in absolute photon number (this should enable determination of excitation energy dependent lifetimes).

■ CONCLUSIONS

The measured and calculated absolute pump−probe signal strengths of fluorescein dianion in basic methanol match within 10% error. The calculations use the decadic molar extinction coefficient, the relative fluorescence spectrum, the pulse spectrum, and the pulse transverse profile from measurements; the expression assumes a vibrationally relaxed electronic two-level system, unity fluorescence quantum yield, and the Condon approximation and can be applied to calculate signal

dx.doi.org/10.1021/jp4019662 | J. Phys. Chem. A 2013, 117, 6332−6345

strength under linear pulse propagation and weak pump conditions. The formula can be applied to polarized experiments because the effect of rotational anisotropy is explicitly included. The absolute measurement of the nonlinear signal presented in this article provides a way to determine the excited state absorption cross-section or excited state quantum yields (and can determine both if a broadband probe is spectrally resolved).

APPENDIX

When the pump and probe can be regarded as collinear, the populations excited by the pump have an exponential depth dependence for every transverse coordinate, and eq 8 is readily solved analytically. If $p_u(\boldsymbol{R}, \nu_u)|_{Z=0}$ is the density of incident pump photons per unit area per unit frequency, then

$$\Delta p_u(\mathbf{R}, \nu_u) = p_u(\mathbf{R}, \nu_u)|_{Z=0}[\exp[-\alpha^0(\nu_u)Z] - 1] \quad \text{(A1)}$$

is the accumulated (integrated from 0 to Z) change in pump photon fluence (a negative number), which is equal in magnitude and opposite in sign to the accumulated density of excited molecules left in the wake of the pump at $T = 0$. The partial derivative of $-\Delta p_u$ with respect to Z is the number of molecules excited by the pump per unit volume per unit pump frequency.

$$\begin{aligned}\Delta n(\mathbf{R}, \nu_u) &= -(\partial \Delta p_u/\partial z) \\ &= p_u(\mathbf{R}, \nu_u)|_{Z=0}\alpha^0(\nu_u)\cdot\exp[-\alpha^0(\nu_u)Z]\end{aligned} \quad \text{(A2)}$$

The change in number density in each excited sublevel j may be calculated by recognizing that each absorption channel is independently absorbing photons at a rate proportional to nB, where n is number density and B is the Einstein B coefficient. For stimulated emission, the photon absorption rate is negative. The net sum of absorption and stimulated emission gives the net depletion of photons[63] (as in the attenuation coefficient of eq 2) and the corresponding net excitation of molecules. Thus, the fraction transferred to level j from level i through either absorption or stimulated emission is

$$n_i^0|\sigma_{ij}(\nu)|/\sum_{k,l} n_k^0\sigma_{k,l}(\nu) = n_i^0|\sigma_{ij}(\nu)|/\alpha^0(\nu) \quad \text{(A3)}$$

The absolute value of the cross section arises because, regardless of whether photons are absorbed (positive cross section) or emitted (negative cross section), molecules are transferred to the final state of the transition. For electronic transitions, the initial excited state molecular number density n_j^0 is usually zero so that the pump does not stimulate emission. Multiplying eq A2 by eq A3, the change in number density in level $j \neq i$, caused by transitions from i to j through pump fluence $p_u(\boldsymbol{R},\nu_u)$ per unit frequency is

$$\Delta n_{ij}(\mathbf{R}, \nu_u) = p_u(\mathbf{R}, \nu_u)|_{Z=0}\, n_i^0|\sigma_{ij}(\nu_u)|\exp[-\alpha^0(\nu_u)Z] \quad \text{(A4)}$$

By conservation of the molecular number density, the change in the number of molecules in the initial level i caused by transitions from i to j is $-\Delta n_{ij}(\mathbf{R},\nu_u)$. If there is thermal population in an upper level excited by the pump, both that upper level and the lower level of that transition will experience partially opposing changes in number density.

The treatment is now extended to incorporate the angular and spatial distribution of the change in population on level j, which will be specified by $\Delta n_{ij}(\boldsymbol{R},\boldsymbol{\Theta},\nu_u)$, where $\boldsymbol{R}$ specifies the molecular spatial coordinates in the laboratory frame, $\boldsymbol{\Theta}$ specifies the Euler angles for the molecular axes in the laboratory frame, and ν_u specifies the pump frequency (u is the first letter of "pump" that does not also appear in "probe"). Integration over the angular distribution recovers the total number density deduced from pump pulse photon number depletion:

$$\Delta n_{ij}(\mathbf{R}, \nu_u) = \int \Delta n_{ij}(\mathbf{R}, \boldsymbol{\Theta}, \nu_u)\mathrm{d}\boldsymbol{\Theta} \quad \text{(A5)}$$

$\Delta n_{ij}(\boldsymbol{R},\boldsymbol{\Theta},\nu_u)$ is integrated over the sublevels of j excited at ν_u. The angular distribution of excited molecules is initially aligned to the pump laser polarization. As a result, the probe propagates in a transiently dichroic and birefringent sample. For a linearly polarized pump and a dipolar pump transition, the transient electric susceptibility is like that of a uniaxial crystal,[64] with one principal axis parallel to the pump polarization and two equivalent principal axes perpendicular. Therefore, probe pulses polarized parallel and perpendicular to the pump propagate without change of polarization. Pulses polarized at all other angles should be decomposed into fields along two principal axes, which are propagated separately in amplitude and phase. In such circumstances, a linearly polarized probe can become elliptically polarized. To evaluate the change in absorption parallel and perpendicular to the pump polarization axis, the angular coordinates can be integrated over both the pump and probe interactions, leaving a polarization index f and an anisotropy that depends on the initial (i), intermediate (j,k), and final (l) states. The intermediate states k include the initial state of the pump transition, i (which is depleted), the initially excited state, j (which is populated), and all states connected to either (or both) of these states by relaxation during the time delay T between pump and probe (which may be either populated or depleted). By defining Δn_{ijk} as the change in number density of state k caused by the pump transition from i to j, Δn_{ijk} may be calculated from Δn_{ij} if the relaxation kinetics are known. For linearly polarized pulses and dipole transitions, the effective change (caused by the pump transition from i to j) in the number density of absorbers for the transition from intermediate state k to final state l is

$$\Delta n_{ijkl}(\mathbf{R}, f, \nu_u, T) = \Delta n_{ijk}(\mathbf{R}, \nu_u, T)[1 + f r_{ijkl}(T)] \quad \text{(A6)}$$

where $r_{ijkl}(T)$ is the anisotropy for excitation from level i to level j (pump excitation) and transition between the levels k to l (probe transition), f is determined by the relative pump and probe polarization ($f = 2$ for parallel and $f = -1$ for perpendicular), and T specifies the pump–probe delay. The total change in attenuation coefficient is given by the sum

$$\begin{aligned}\Delta\alpha(\mathbf{R}, \nu_r, f, T) = \sum_{i,j,k,l}\Bigg[\int_0^\infty \Delta n_{ijkl}(\mathbf{R}, f, T, \nu_u) \\ \cdot\sigma_{kl}(\nu_r, T, \nu_u)\mathrm{d}\nu_u\Bigg]\end{aligned} \quad \text{(A7)}$$

where the indices run over the levels.

The treatment here assumes that probe transitions from k can be described by absorption and stimulated emission cross-sections $\sigma_{kl}(T,\nu_u,\nu_r)$ that depend on the final state l, the pump–probe delay, the pump frequency, and the probe frequency (ν_r). This allows inclusion of nonequilibrium correlation between the pumped and probed sublevel populations. In the bilinear pulse propagation limit considered here, the signals from more than one starting state are additive.

dx.doi.org/10.1021/jp4019662 | J. Phys. Chem. A 2013, 117, 6332–6345

AUTHOR INFORMATION

Corresponding Author

*(D.M.J.) Phone: (303) 492-3818. E-mail: david.jonas@colorado.edu.

Present Addresses

[†]Department of Chemistry, University of Washington, Seattle, Washington 98195-1700, United States.

[§]Intel Corporation, Hillsboro, Oregon 97124, United States.

[#]JILA, University of Colorado and National Institute of Standards and Technology, Boulder, Colorado 80309-0440, United States.

Author Contributions

[‡]These authors contributed equally to this work.

Notes

The authors declare no competing financial interest.

ACKNOWLEDGMENTS

D.M.J. thanks John Wright for support and encouragement since their first meeting 14 years ago. We thank both anonymous referees for helpful comments. This work was funded by the Division of Chemical Sciences, Geosciences, and Biosciences, Office of Basic Energy Sciences of the U.S. Department of Energy through Grant DE-FG02-07ER15912.

REFERENCES

(1) Norrish, R. G. W.; Porter, G. Chemical Reactions Produced by Very High Light Intensities. *Nature* **1949**, *164*, 658−658.

(2) Herzberg, G.; Shoosmith, J. Spectrum and Structure of the Free Methylene Radical. *Nature* **1959**, *183*, 1801−1802.

(3) Bowers, P. G.; Porter, G. Quantum Yields of Triplet Formation in Solutions of Chlorophyll. *Proc. R. Soc. London, Ser. A* **1967**, *296*, 435−441.

(4) Kuhn, H. J.; Braslavsky, S. E.; Schmidt, R. Chemical Actinometry. *Pure Appl. Chem.* **2004**, *76*, 2105−2146.

(5) Fleming, G. R. *Chemical Applications of Ultrafast Spectroscopy*; Oxford University Press: New York, 1986; Vol. *13*.

(6) Menzel, R.; Rapp, W. Excited Singlet-Absorptions and Triplet-Absorptions of Pentaphene. *Chem. Phys.* **1984**, *89*, 445−455.

(7) Muller, A.; Schulzhennig, J.; Tashiro, H. Excited-State Absorption of 1,3,3,1′,3′,3′-Hexamethylindotricarbocyanine Iodide: Quantitative Study by Ultrafast Absorption Spectroscopy. *Appl. Phys.* **1977**, *12*, 333−339.

(8) Bernstein, R. B.; Zewail, A. H. Femtosecond Real-Time Probing of Reactions. III. Inversion to the Potential from Femtosecond Transition State Spectroscopy Experiments. *J. Chem. Phys.* **1989**, *90*, 829−842.

(9) Swatton, S. N. R.; Welford, K. R.; Hollins, R. C.; Sambles, J. R. A Time Resolved Double Pump-Probe Experimental Technique to Characterize Excited-State Parameters of Organic Dyes. *Appl. Phys. Lett.* **1997**, *71*, 10−12.

(10) Swatton, S. N. R.; Welford, K. R.; Till, S. J.; Sambles, J. R. Nonlinear Absorption of a Carbocyanine Dye 1,1′,3,3,3′,3′-Hexamethylindotricarbocyanine Iodide Using a Z-Scan Technique. *Appl. Phys. Lett.* **1995**, *66*, 1868−1870.

(11) Webster, S.; Odom, S. A.; Padilha, L. A.; Przhonska, O. V.; Peceli, D.; Hu, H. H.; Nootz, G.; Kachkovski, A. D.; Matichak, J.; Barlow, S.; et al. Linear and Nonlinear Spectroscopy of a Porphyrin−Squaraine−Porphyrin Conjugated System. *J. Phys. Chem. B* **2009**, *113*, 14854−14867.

(12) Klán, P.; Wirz, J. *Photochemistry of Organic Compounds*; Wiley: Chichester, U.K., 2009.

(13) Jonas, D. M.; Lang, M. J.; Nagasawa, Y.; Joo, T.; Fleming, G. R. Pump−Probe Polarization Anisotropy Study of Femtosecond Energy Transfer within the Photosynthetic Reaction Center of *Rhodobacter sphaeroides* R26. *J. Phys. Chem.* **1996**, *100*, 12660−12673.

(14) McGuire, J. A.; Joo, J.; Pietryga, J. M.; Schaller, R. D.; Klimov, V. I. New Aspects of Carrier Multiplication in Semiconductor Nanocrystals. *Acc. Chem. Res.* **2008**, *41*, 1810−1819.

(15) Paci, I.; Johnson, J. C.; Chen, X.; Rana, G.; Popovic, D.; David, D. E.; Nozik, A. J.; Ratner, M. A.; Michl, J. Singlet Fission for Dye-Sensitized Solar Cells: Can a Suitable Sensitizer Be Found? *J. Am. Chem. Soc.* **2006**, *128*, 16546−16553.

(16) Einstein, A. Zur Quantentheorie der Strahlung. *Phys. Z* **1917**, *18*, 121−128.

(17) Einstein, A. On the Quantum Theory of Radiation [English Translation of *Phys. Z.* **18** (1917) 121]. In *Sources of Quantum Mechanics*; van der Waerden, B. L., Ed.; Dover: New York, 1967; pp 63−77.

(18) Demtröder, W. *Laser Spectroscopy*, 2nd ed.; Springer-Verlag: New York, 1982.

(19) Hilborn, R. C. Einstein Coefficients, Cross Sections, *f* Values, Dipole Moments, and All That. *Am. J. Phys.* **1982**, *50*, 982−986.

(20) Allen, L.; Eberly, J. H. *Optical Resonance and Two-Level Atoms*; Dover Publications, Inc.: New York, 1987.

(21) Kinrot, O.; Prior, Y. Nonlinear Interaction of Propagating Short Pulses in Optically Dense Media. *Phys. Rev. A* **1995**, *51*, 4996−5007.

(22) Belabas, N.; Jonas, D. M. Fourier Algorithm for Four-Wave Mixing Signals from Optically Dense Systems with Memory. *Opt. Lett.* **2004**, *29*, 1811−1813.

(23) Hecht, E. *Optics*, 2nd ed.; Addison-Wesley: Reading, MA, 1990.

(24) Siegman, A. E. Bragg Diffraction of a Gaussian Beam by a Crossed-Gaussian Volume Grating. *J. Opt. Soc. Am.* **1977**, *67*, 545−550.

(25) Ladenburg, R. Der quantentheoretische Deutung der Zahl der Dispersionselektronen. *Z. F. Phys.* **1921**, *4*, 451−468.

(26) Ladenburg, R. The Quantum-Theoretical Interpretation of the Number of Dispersion Electrons [English Translation of *Z. F. Phys.* **4** (1921) 451−468]. In *Sources of Quantum Mechanics*; van der Waerden, B. L., Ed.; Dover: New York, 1967; pp 139−157.

(27) Widom, B. *Statistical Mechanics: A Concise Introduction for Chemists*: Cambridge University Press: Cambridge, U.K., 2002.

(28) Mukamel, S. Femtosecond Optical Spectroscopy: A Direct Look at Elementary Chemical Events. *Annu. Rev. Phys. Chem.* **1990**, *41*, 647−681.

(29) Jonas, D. M.; Fleming, G. R. Vibrationally Abrupt Pulses in Pump−Probe Spectroscopy. In *Ultrafast Processes in Chemistry and Photobiology*; El-Sayed, M. A., Tanaka, I., Molin, Y., Eds.; Blackwell Scientific: Oxford, U.K., 1995; pp 225−256.

(30) Ulness, D. J.; Kirkwood, J. C.; Albrecht, A. C. Competitive Events in Fifth Order Time Resolved Coherent Raman Scattering: Direct Versus Sequential Processes. *J. Chem. Phys.* **1998**, *108*, 3897−3902.

(31) Blank, D. A.; Kaufman, L. J.; Fleming, G. R. Fifth Order Two Dimensional Raman Spectra of CS_2 Are Dominated by Third Order Cascades. *J. Chem. Phys.* **1999**, *111*, 3105−3114.

(32) Wright, J. C. Coherent Multidimensional Vibrational Spectroscopy. *Int. Rev. Phys. Chem.* **2002**, *21*, 185−255.

(33) Schriever, C.; Pugliesi, I.; Riedle, E. A Novel Ultra-Broadband Transient Spectrometer with Microsecond Measurement Range Based on a Supercontinuum Fiber Laser. *Appl. Phys. B: Laser Opt.* **2009**, *96*, 247−250.

(34) Hybl, J. D.; Albrecht Ferro, A.; Jonas, D. M. Two Dimensional Fourier Transform Electronic Spectroscopy. *J. Chem. Phys.* **2001**, *115*, 6606−6622.

(35) Yetzbacher, M. K.; Belabas, N.; Kitney, K. A.; Jonas, D. M. Propagation, Beam Geometry, and Detection Distortions of Peak Shapes in Two-Dimensional Fourier Transform Spectra. *J. Chem. Phys.* **2007**, *126*, art. no. 044511.

(36) Martin, M. M.; Lindqvist, L. pH-Dependence of Fluorescein Fluorescence. *J. Lumin.* **1975**, *10*, 381−390.

(37) Förster, T. 10th Spiers Memorial Lectrures: Transfer Mechanisms of Electronic Excitation. *Discuss. Faraday Soc.* **1959**, 7−17.

(38) Seybold, P. G.; Gouterman, M.; Callis, J. Calorimetric, Photometric and Lifetime Determinations of Fluorescence Yields of Fluorescein Dyes. *Photochem. Photobiol.* **1969**, *9*, 229−242.
(39) Assuming uniform flow, this corresponds to a linear velocity of 1.56 m/s in the 0.200 mm × 8 mm rectangular cell. Approximating the rectangular cross-section with an ellipse, laminar flow calculations yield an average flow velocity of 2.67 m/s. The slowest 10% of molecules (near the boundary of the flow cell) yield an average velocity of 0.40 m/s (40 μm in 100 microsecond).
(40) Landau, L. D.; Lifshitz, E. M. *Fluid Mechanics*, 2nd ed.; Pergamon Press: New York, 1987.
(41) Strickler, S. J.; Berg, R. A. Relationship between Absorption and Fluorescence Lifetime of Molecules. *J. Chem. Phys.* **1962**, *37*, 814−822.
(42) Yu, A.; Tolbert, C. A.; Jonas, D. M. Solvatochromism and Solvation Dynamics of Structurally Related Cyanine Dyes. *J. Phys. Chem. A* **2002**, *106*, 9407−9419.
(43) Magde, D.; Wong, R.; Seybold, P. G. Fluorescence Quantum Yields and Their Relation to Lifetimes of Rhodamine 6G and Fluorescein in Nine Solvents: Improved Absolute Standards for Quantum Yields. *Photochem. Photobiol.* **2002**, *75*, 327−334.
(44) Cho, B. M.; Walker, R. C.; Amer, H.; Mercer, I.; Klug, D. R.; Gould, I. R. Effect of Adiabaticity on Electron Dynamics in Zinc Myoglobin. *J. Phys. Chem. B* **2005**, *109*, 5954−5961.
(45) Piel, J.; Riedle, E.; Gundlach, L.; Ernstorfer, R.; Eichberger, R. Sub-20 fs Visible Pulses with 750 nJ Energy from a 100 kHz Noncollinear Optical Parametric Amplifier. *Opt. Lett.* **2006**, *31*, 1289−1291.
(46) Siegman, A. E. *Lasers*; University Science Books: Mill Valley, CA, 1986.
(47) Berg, M. A.; Zhang, Y. Ultrafast Dichroism Spectroscopy of Anthracene in Solution. III. Nonpolar Solvation Dynamics in Benzyl Alcohol. *J. Chem. Phys.* **2001**, *115*, 4231−4238.
(48) Horng, M. L.; Gardecki, J. A.; Papazyan, A.; Maroncelli, M. Subpicosecond Measurements of Polar Solvation Dynamics: Coumarin 153 Revisited. *J. Phys. Chem.* **1995**, *99*, 17311−17337.
(49) Arik, M.; Çelebi, N.; Onganer, Y. Fluorescence Quenching of Fluorescein with Molecular Oxygen in Solution. *J. Photochem. Photobiol., A* **2005**, *170*, 105−111.
(50) Von Jena, A.; Lessing, H. E. Rotational Diffusion of Dyes in Solvents of Low Viscosity from Transient-Dichroism Experiments. *Chem. Phys. Lett.* **1981**, *78*, 187−193.
(51) Meyer, Y. H.; Pittman, M.; Plaza, P. Transient Absorption of Symmetrical Carbocyanines. *J. Photochem. Photobiol., A* **1998**, *114*, 1−21.
(52) Joo, T.; Jia, Y.; Yu, J.-Y.; Lang, M. J.; Fleming, G. R. Third-Order Nonlinear Time Domain Probes of Solvation Dynamics. *J. Chem. Phys.* **1996**, *104*, 6089−6108.
(53) de Boeij, W. P.; Pshenichnikov, M. S.; Wiersma, D. A. System-Bath Correlation Function Probed by Conventional and Time-Gated Stimulated Photon Echo. *J. Phys. Chem.* **1996**, *100*, 11806−11823.
(54) Passino, S. A.; Nagasawa, Y.; Joo, T.; Fleming, G. R. Three-Pulse Echo Peak Shift Studies of Polar Solvation Dynamics. *J. Phys. Chem. A* **1997**, *101*, 725−731.
(55) Yartsev, A.; Alvarez, J.-L.; Åberg, U.; Sundström, V. Overdamped Wavepacket Motion Along a Barrierless Potential Energy Surface in Excited State Isomerization. *Chem. Phys. Lett.* **1995**, *243*, 281−289.
(56) Hunt, P. A.; Robb, M. A. Systematic Control of Photochemistry: The Dynamics of Photoisomerization of a Model Cyanine Dye. *J. Am. Chem. Soc.* **2005**, *127*, 5720−5726.
(57) Wei, Z.; Nakamura, T.; Takeuchi, S.; Tahara, T. Tracking of the Nuclear Wavepacket Motion in Cyanine Photoisomerization by Ultrafast Pump−Dump−Probe Spectroscopy. *J. Am. Chem. Soc.* **2011**, *133*, 8205−8210.
(58) Mohanty, J.; Palit, D. K.; Mittal, J. Photophysical Properties of Two Infrared Laser Dyes—IR-144 and IR-140: A Picosecond Laser Flash Photolysis Study. *Proc. Indian Natl. Sci. Acad., Part A* **2000**, *66*, 303−618.
(59) Lougnot, D.-J.; Goldschmidt, C. R. Photoionization of Fluorescein via Excited Triplet and Singlet States. *J. Photochem.* **1980**, *12*, 215−224.
(60) Peterson, O. G.; Webb, J. P.; McColgin, W. C.; Eberly, J. H. Organic Dye Laser Threshold. *J. Appl. Phys.* **1971**, *42*, 1917−1928.
(61) Cho, B.; Tiwari, V.; Jonas, D. M. Simultaneous All-Optical Determination of Molecular Concentration and Extinction Coefficient. *Anal. Chem.* **2013**, DOI: dx.doi.org/10.1021/ac400656r.
(62) Jonas, D. M. Two-Dimensional Femtosecond Spectroscopy. *Annu. Rev. Phys. Chem.* **2003**, *54*, 425−463.
(63) Van Vleck, J. H. Absorption of Radiation by Multiply Periodic Orbits, and its Relation to the Correspondence Principle and the Rayleigh-Jeans Law. Part I. Some Extensions of the Correspondence Principle. *Phys. Rev.* **1924**, *24*, 330−346.
(64) Yariv, A. *Quantum Electronics*, 2nd ed.; John Wiley and Sons: New York, 1975.